

Optimization of Pt-Oxygen-Containing-Species Anodes for Ethanol Oxidation Reaction: High Performance of Pt-AuSnO_x Electrocatalyst

Sheng Dai^{1,2,7}, Tzu-Hsi Huang^{1,3,7}, Po-Cheng Chien⁴, Cheng-An Lin³, Chen-Wei

Liu⁵, Sheng-Wei Lee³, Jeng-Han Wang^{4,*}, Kuan-Wen Wang^{2,3,*}, Xiaoqing Pan^{2,6,7*}

¹ Key Laboratory for Advanced Materials and Feringa Nobel Prize Scientist Joint Research Center, Institute of Fine Chemicals, School of Chemistry & Molecular Engineering, East China University of Science and Technology, Shanghai 200237, P.R. China

² Department of Materials Science and Engineering, University of California-Irvine, Irvine, California 92697, United States

³ Institute of Materials Science and Engineering, National Central University, Taoyuan 320, Taiwan

⁴ Department of Chemistry, National Taiwan Normal University, Taipei 116, Taiwan

⁵ Green Energy and Environment Research Laboratories, Industrial Technology Research Institute, Hsinchu 310, Taiwan

⁶ Department of Physics and Astronomy, University of California-Irvine, Irvine, California 92697, United States

⁷ Irvine Materials Research Institute (IMRI), University of California, Irvine, California 92697, United States

1. METHODS

1.1 Computational Method

The computational work was performed by Vienna Ab initio Simulation Package (VASP).²⁵⁻²⁷ at the GGA-PW91 level, the generalized gradient approximation²⁸ with Perdew-Wang 1991 formulation.²⁹ Valance electrons were expanded by planewave basis at 600-eV cutoff energy and core electrons were treated with cost-effective pseudopotentials with projector-augmented wave method (PAW).^{30, 31} The Brillouin Zone integration was sampled by Monkhorst-Pack scheme³² with the k-point interval at 0.05×2 ($1/\text{\AA}$). The structural optimization and energetic calculation employed quasi-Newton method with an energetic convergence of 1×10^{-4} eV and a gradient convergence of 1×10^{-2} eV. The transition state searching and activation barrier calculation were obtained by Nudged Elastic Band (NEB) method³³ at the same convergence criterions.

Pt-OCS electrodes were modeled based on the Pt(111) surface, which is widely applied in the study of Pt-based electro-catalytic reactions^{9, 34-35}; the Pt(111) supercell was constructed by a five-layer 4×4 Pt slab, in which the top three layers were free to relax and the bottom two ones were fixed at the computed lattice constants, and an equivalent five-layer vacuum space to limit the artificial interaction between the distinct slabs. Foreign atoms of Sn, Co, Ni, Cu, Rh, Pd, Ir, and Au were decorated on Pt(111) surface, and then, O atom was further covered on the foreign elements to model their oxygen containing species.

1.2 Catalyst Synthesis

Carbon-supported Pt, Pt-AuO_x, Pt-SnO_x and Pt-AuSnO_x nanorod catalysts with metal loading of 20 wt. % and Pt/Au/Sn atomic ratio of 100/0/0, 70/30/0, 70/0/30, and 70/15/15 were prepared through a formic acid reduction method (FAM). First, the aqueous solution of H₂PtCl₆ (Alfa Aesar) was mixed with 50 mg of carbon black

(Vulcan XC-72R) that has been dispersed in deionized water, and then reduced by formic acid (98 %) at 278 K for more than 9 days to synthesize the carbon-supported Pt nanorods. As for the Pt-OCS electrocatalysts, the additional metal precursor (HAuCl₄, SnCl₂, or HAuCl₄ and SnCl₂ with desired stoichiometric ratios) was added into the solution and reduced by formic acid for another 3 days, respectively, to decorate OCS (AuO_x, SnO_x, and AuSnO_x) on the Pt nanorod surface. Then, the prepared Pt-OCS catalysts were washed and dried at 340 K for 1 day.

1.3 Materials Characterization

Morphology and structural information of the Pt-OCS catalysts were characterized through aberration-corrected scanning transmission electron microscopy (AC-STEM), performed on a JEOL Grand ARM300F equipped with two spherical aberration correctors. High angle annular dark field (HAADF)-STEM images were recorded using a convergence semi angle of 22 mrad, and inner- and outer collection angles of 83 and 165 mrad, respectively. Energy dispersive X-ray spectroscopy (EDS) was carried out using JEOL dual EDS detectors and a specific high count analytic TEM holder. Moreover, transmission electron microscope (TEM) was also carried out for additional morphology characterization.

Crystalline information of the Pt-OCS catalysts was characterized via X-ray diffraction (XRD, Rigaku) using Cu K α , operated at 40 kV and 40 mA. The catalysts were scanned in a 2θ range from 20° to 80° at a scan rate of 0.124°/s. Atomic compositions of the catalysts were further determined by inductively coupled plasma optical emission spectrometry (ICP-OES, Agilent 725). Surface chemical states of the Pt-OCS catalysts were analyzed by X-ray photoelectron spectroscopy (XPS, Thermo VG Scientific Sigma Probe) using an Al K α radiation at a voltage of 20 kV and a current of 30 mA.

X-ray absorption spectroscopy (XAS) was carried out in transmission or fluorescence mode at the BL01C1 and 17C beamlines at the National Synchrotron Radiation Research Center (NSRRC). The incident beam was monochromated using a double crystal monochromator equipped with a Si (111) crystal. A Si monochromator was employed to adequately select the energy with a resolution $\Delta E/E$ better than 10^{-4} at the Pt L_2 -edge (13273 eV) and Pt L_3 -edge (11564 eV). Based on the Pt L_2 and L_3 spectra, the fractional change in the number of d-band vacancies relative to the reference material (f_d) can be estimated according to the following equation:

$$f_d = \frac{\Delta A_3 + 1.1\Delta A_2}{(A_3 + 1.1A_2)_r} \quad (1)$$

where ΔA_2 and ΔA_3 are expressed by

$$\Delta A_2 = A_{2s} - A_{2r} \text{ and } \Delta A_3 = A_{3s} - A_{3r} \quad (2)$$

The terms A_2 and A_3 , which represented the areas under L_{II} and L_{III} absorption edges of the sample (s) and reference (r) material as well as the calculated H_{Ts} , were evaluated from band structure calculations. The d-band vacancies of Pt in the sample can be evaluated using the equation using the relation. The value of infilled d-states in the reference material (H_{Tr}) had been evaluated from band structure calculations to be 0.3.

$$H_{Ts} = (1 + f_d)H_{Tr} \quad (3)$$

1.4 CO Stripping Experiment

CO stripping tests were performed with potentiostat (CHI 612E) and a three-electrode cell. A glass carbon electrode, a Pt wire and a Ag/AgCl electrode were used as the work, counter and reference electrodes, respectively. The adsorption of CO on the catalysts surface was performed by purging CO into 0.5 M H_2SO_4 at 0.05 V for 30 min. Then the CO stripping voltammetry was measured between -0.10 and 1.20 V in N_2 saturated 0.5 M H_2SO_4 solution at a scan rate of 50 mVs⁻¹.

1.5 Electrochemical Measurements

Electrochemical measurements were conducted on a CH Instruments Model 611c device. The counter and reference electrodes were Pt plate and silver/silver chloride electrode (SSCE). All potentials in this study were referred to the normal hydrogen electrode (NHE), respectively. 5 mg of the catalysts in 1 ml IPA and 50 μ l Nafion solution (5 wt. %, DuPont) were ultrasonically dispersed and dropped on a glass carbon electrode as a working electrode.

Cyclic voltammograms (CV) were swept between 0 and 1.4 V (vs. NHE) at the rate of 50 mVs⁻¹ in 0.5 M H₂SO₄ purged with N₂ for 30 minutes to ensure the electrolyte is N₂-saturated. The ECSA by H-adsorption (ECSA) was calculated by integrating the areas of hydrogen desorption at 0-0.4 V (Q). The values were obtained from the following equation:

$$\text{ECSA} = \frac{Q}{[\text{Pt}] \times 0.21} \quad (4)$$

where 0.21 (mC/m²) is the charge required to oxidize a monolayer of H₂ on Pt active sites. For the EOR activity, the CVs were swept between 0 to 1.2 V (vs. NHE) with a scanning rate of 2 mVs⁻¹. The durability test of the EOR catalysts was measured at a constant voltage of 0.6 V (vs. NHE) for 2 hours by chronoamperometric (CA), and the electrolyte for CV and CA was both N₂-saturated 0.5 M H₂SO₄ containing 1.0 M C₂H₅OH.

2. Results and Discussion for Supporting Information

2.1 Quantitative analysis of XRD result

X-ray diffraction was performed on the Pt-OCS catalysts, and the quantitative result is presented in Table S3. Here, intensities of the diffraction peaks of Pt, e.g., (111),

(200), and (220) peaks are listed. Meanwhile, ratios of the peak intensities as compared to the (111) peak are used to measure the exposed facets of the nanorod surface.

According to the reference spectra of JCPDS Pt (using polycrystalline Pt), the values of $I_{(200)}/I_{(111)}$ (0.53) and $I_{(222)}/I_{(111)}$ (0.31) reflect the structure factor F_{hkl} and the standard peak intensity ratios of fcc Pt. In contrast, as for the three Pt-OCS catalysts (Pt-AuO_x, Pt-SnO_x, and Pt-AuSnO_x), it is clear that both these intensity ratios ($I_{(200)}/I_{(111)}$ and $I_{(222)}/I_{(111)}$) dropped down about 30%, indicating that (111) peak intensity became much stronger in our as-synthesized catalysts. This evidence demonstrates that more (111) surface facets are exposed in our Pt-based nanorod catalysts.

2.2 CO stripping analysis

We carried out the CO-stripping experiment for the as-prepared Pt, Pt-AuO_x, Pt-SnO_x, and Pt-AuSnO_x nanorod catalysts, and the result demonstrates the superior CO poisoning tolerance of Pt-AuSnO_x catalyst, as shown in Figure S6. Notably, CO-stripping peaks of pure Pt nanorods are located at 0.65 and 0.9 V, working as the reference for comparison. As for Pt-AuO_x catalyst, the two peaks show a slight shift to the lower potential region, indicating the modification of Pt d-band through the decoration of AuO_x. Then, as for the two Sn-containing catalysts, Pt-SnO_x and Pt-AuSnO_x, their CO-stripping peaks shift to even lower potential region (at 0.4 and 0.75 V for both), highlighting the significant promotion effect for the oxidation of adsorbed CO. This experimental evidence demonstrates the superior CO poisoning tolerance of the two Sn-containing Pt-OCS catalysts and is consistent with our DFT calculation result of $E_{\text{ads}}(\text{CO})$.

Table S1. E_{seg} , $E_{\text{ads}}(\text{O})$, and $E_{\text{ads}}(\text{H})$ on Pt-OCS catalysts (in eV). The last column shows the reference value of pure Pt.

| | SnO | CoO | NiO | CuO | RhO | PdO | IrO | AuO | Pt |
|----------------------------|------------|------------|------------|------------|------------|------------|------------|------------|-----------|
| E_{seg} | 4.40 | -2.39 | -2.11 | -1.33 | -1.51 | -0.16 | -1.52 | -1.13 | 0.00 |
| $E_{\text{ads}}(\text{O})$ | -4.84 | -6.94 | -5.81 | -4.80 | -5.72 | -4.35 | -6.01 | -3.75 | -3.96 |
| $E_{\text{ads}}(\text{H})$ | -3.01 | -2.68 | -3.26 | -3.88 | -2.96 | -3.65 | -2.70 | -4.02 | -2.74 |

Table S2. Bader charges of Au and Sn in Pt-OCS electrodes.

| | Pt-AuO | Pt-SnO | Pt-AuSnO |
|-----------|---------------|---------------|-----------------|
| Au | 0.35 | | 0.33 |
| Sn | | 2.23 | 2.91 |
| O | -0.74 | -1.63 | -1.42 |

Table S3. Energetics of E_a and ΔE (in eV) for C-C bond cleavage step on Pt, Pt-SnO and Pt-AuSnO.

| | | Pt | Pt-SnO | Pt-AuSnO |
|---|------------|-----------|---------------|-----------------|
| CH₃CO → CH₃+CO | E_a | 1.90 | 1.81 | 2.24 |
| | ΔE | -0.26 | -0.14 | -0.06 |

Table S4. X-ray diffraction analysis of JCPDS Pt and as-synthesized Pt-OCS catalysts. Peak intensities are normalized using the intensity of (111) peak as reference.

| | (111) | (200) | | (220) | |
|-----------------------|-----------------------|-----------------------|-----------------------|-----------------------|-----------------------|
| | Intensity(<i>I</i>) | Intensity(<i>I</i>) | $I_{(200)}/I_{(111)}$ | Intensity(<i>I</i>) | $I_{(222)}/I_{(111)}$ |
| JCPDS Pt | 100 | 53 | 0.53 | 31 | 0.31 |
| Pt | 1813 | 666 | 0.37 | 389 | 0.21 |
| Pt-AuO _x | 1660 | 480 | 0.29 | 330 | 0.20 |
| Pt-SnO _x | 1847 | 646 | 0.35 | 292 | 0.16 |
| Pt-AuSnO _x | 1422 | 426 | 0.30 | 288 | 0.20 |

Table S5. Comparison of EOR activity between Pt-AuSnO_x catalyst and other Pt-Sn based ternary and PtAu catalysts taken from literature.

| Samples | Electrolyte | Onset Potential (V) | Mass Activity (mA/mg _{Pt}) | Ref. |
|-----------------------------|--|---------------------|---|-------------------|
| PtRhSn | 0.5 M EtOH + 0.5 M H ₂ SO ₄ | 0.29 | MA _{0.6} = 46.8 MA _{0.45} = 21.7 MA _{0.45-5 min} = 4.4 | Ref. 5 |
| PtRhSn | 0.5 M EtOH + 0.1 M HClO ₄ | 0.35 | MA _{0.45} = 12.0 MA _{0.45-17 min} = 2.7 MA _{max} = 119.2 | Ref. 17 |
| Pt ₃ Au | 0.5 M EtOH + 0.5 M H ₂ SO ₄ | 0.13 | MA _{0.6} = 55.2 MA _{0.6-67 min} = 28.6 MA _{max} = 80.1 | Ref. 18 |
| Pt ₃ RhSn | 0.5 M EtOH + 0.1 M HClO ₄ | 0.29 | MA _{0.45} = 23.4 MA _{0.45-2 hr} = 5.0 | Ref. 19 |
| PtSnFe | | 0.18 | MA _{0.4} = 20.5 MA _{0.4-30 min} = 11.8 | |
| PtSnNi | 1 M EtOH + 0.05 M H ₂ SO ₄ | 0.19 | MA _{0.4} = 17.3 MA _{0.4-30 min} = 11.8 | Ref. 20 |
| PtSnPd | | 0.19 | MA _{0.4} = 16.5 MA _{0.4-30 min} = 9.6 | |
| PtSnRu | | 0.24 | MA _{0.4} = 5.5 MA _{0.4-30 min} = 2.8 | |
| PtSnRu | 1M EtOH + 0.5 M H ₂ SO ₄ | 0.23 | MA _{0.4} = 6.1 MA _{0.4-2 h} = 1.6 MA _{max} = 43.2 | Ref. 21 |
| Pt-AuSnO_x | 1M EtOH + 0.5 M H₂SO₄ | 0.24 | MA_{0.45} = 42.4 MA_{0.6} = 63.6 MA_{0.6-2 hr} = 24.8 MA_{max} = 302.0 | This study |

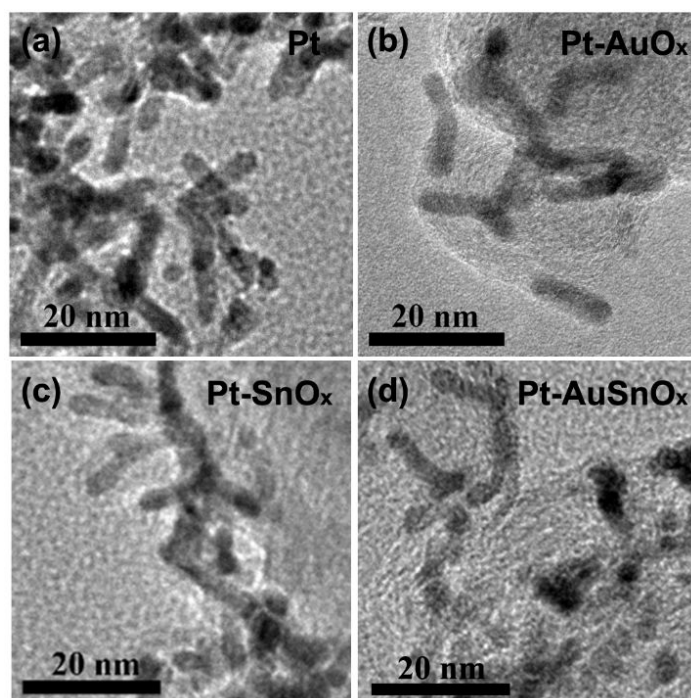


Figure S1. HRTEM micrographs of as-prepared (a) Pt, (b) Pt-AuO_x, (c) Pt-SnO_x, and (d) Pt-AuSnO_x catalysts.

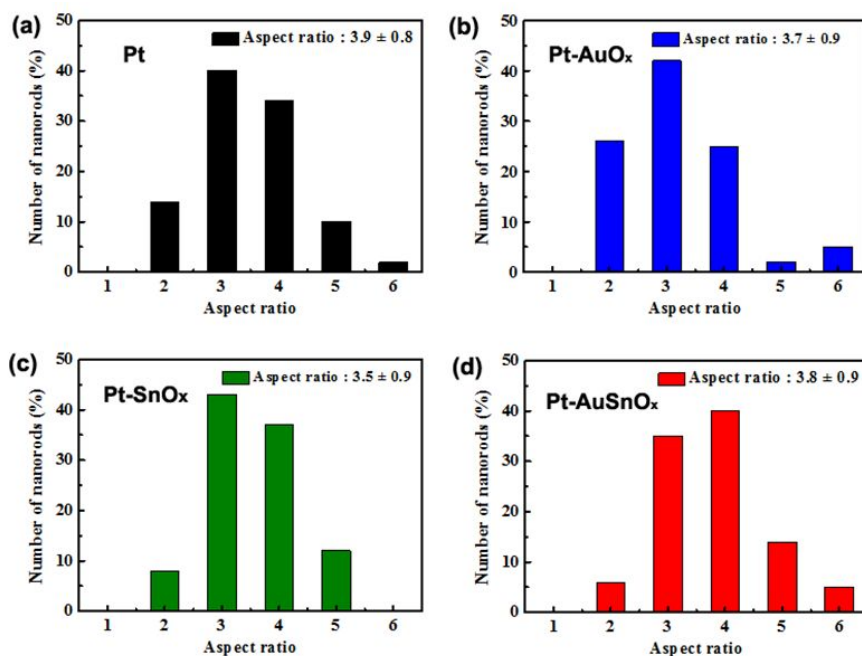


Figure S2. Statistic distribution of the aspect ratios of the as-synthesized (a) Pt, (b) Pt-AuO_x, (c) Pt-SnO_x, and (d) Pt-AuSnO_x nanorod catalysts.

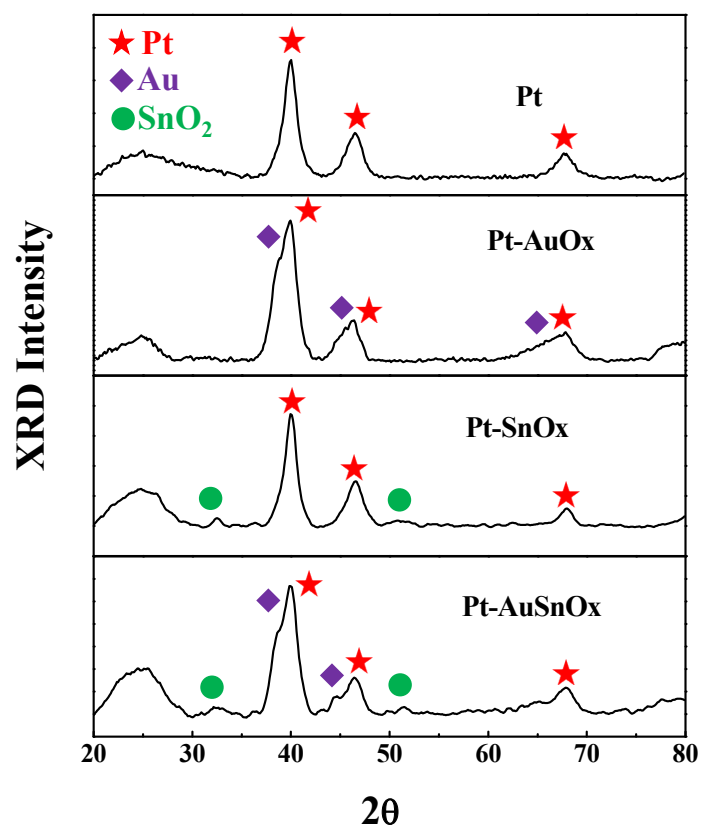


Figure S3. XRD patterns of Pt, Pt-AuO_x, Pt-SnO_x, and Pt-AuSnO_x catalysts.

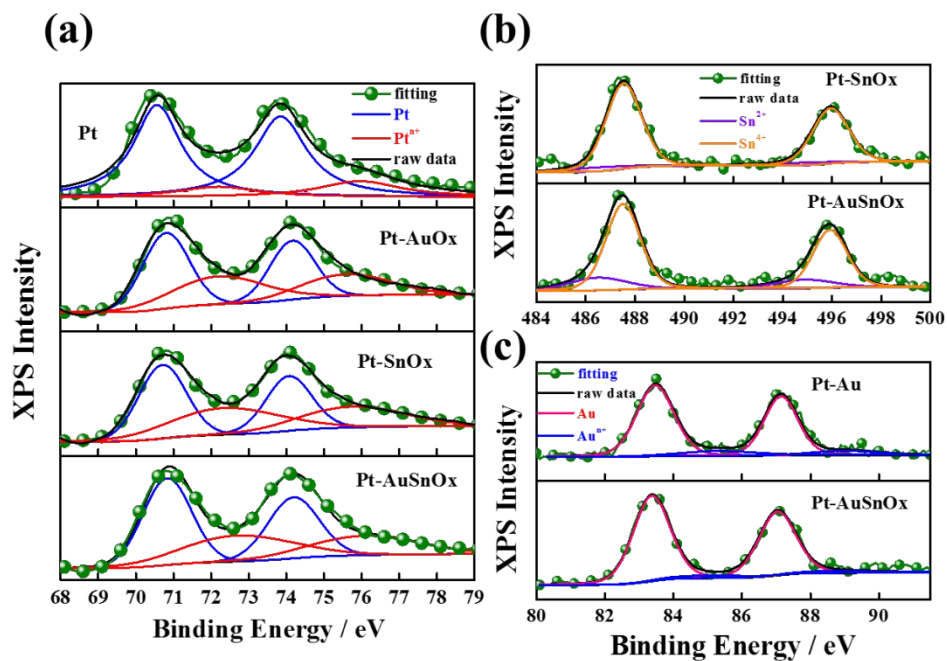


Figure S4. (a) XPS Pt 4f, (b) XPS Sn 3d, and (c) XPS Au 4f spectra of Pt, Pt-AuO_x, Pt-SnO_x, and Pt-AuSnO_x catalysts.

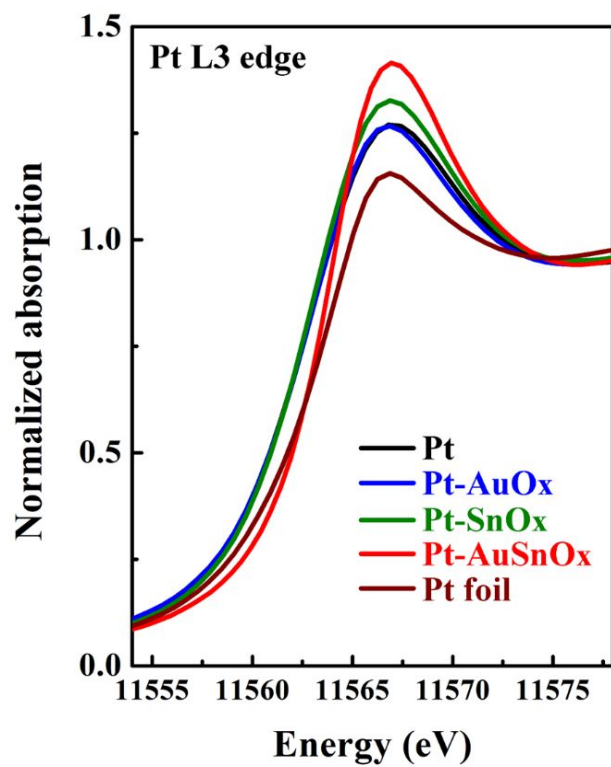


Figure S5. XANES at Pt L₃ edge of reference Pt foil, Pt, Pt-AuO_x, Pt-SnO_x, and

Pt-AuSnO_x catalysts.

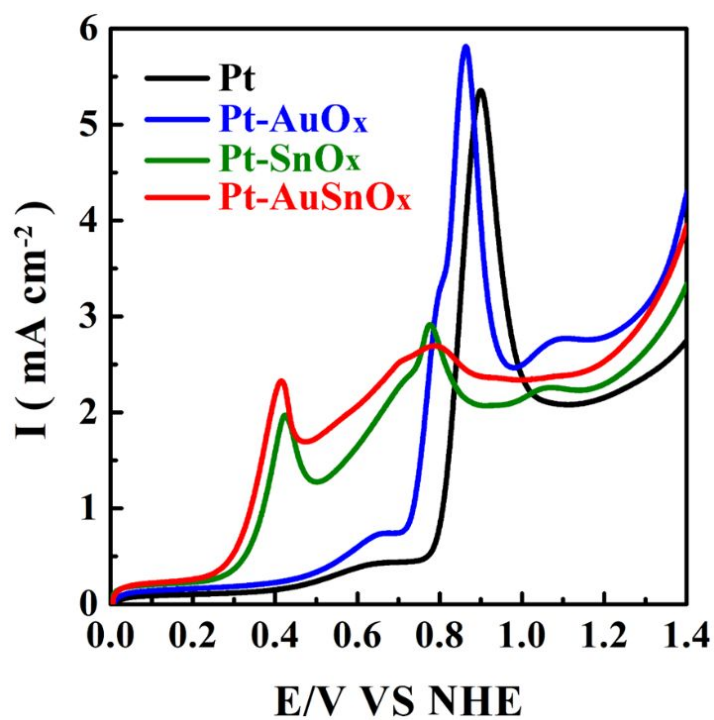


Figure S6. CO-stripping results of Pt, Pt-AuO_x, Pt-SnO_x, and Pt-AuSnO_x catalysts.